# Classification of Multiple Electromechanical Faults in BLDC Motors Using Neural Networks and Optimization Algorithms

Faezeh Hosseini[1], Mostafa Abedi[1,*], Saba Mohammad Hosseini[1]

[1] *Electrical Engineering Department, Shahid Beheshty University, Tehran, Iran*

| ARTICLEINFO | ABSTRACT |
|---|---|
| <br><br> | Fault detection and classification of brushless DC motors (BLDCM) is considered in this paper. A novel solution is introduced to diagnose multiple electromechanical faults that includes the stator inter-turn, the rotor dynamic imbalance, the rotor static imbalance, and different combinations of them. The current signal of the BLDCM is used together with the motor torque and the motor speed to achieve the classification of a wide range of defects. The fault features of the measured signals are extracted using packet wavelet transform (PWT). These features which include the energy, in the two modes of BLDCM operation: without load and with load, are used as input data for the radial basis function (RBF) neural network. Therefore, the designed algorithm maintains its efficiency in all operating conditions of the BLDCM. Besides, by the combination of the mentioned algorithms, the relationship between the fault types and different affected parameters of the measured signals are obtained more precisely. The neural network weights are updated by the particle swarm optimization (PSO) and the genetic algorithm (GA) that improve the convergence speed and provide better flexibility for local problems. Finally, the effectiveness of the proposed methods is validated by comparing the results obtained for different combinations of the neural networks and optimization methods. |

## 1. Introduction

BLDCM is found to be great choices in different applications due to their efficiency, reliability, higher lifetime, lower noise, and energy consumption. Different defects may happen in BLDCM which is due to electromechanical or electronic board faults. Electromechanical faults, in turn, are classified into stator, rotor and, magnetic defects. These defects may lead to important problems and reduce the ability, efficiency, or system safety. Accordingly, the fault detection problem in these motors is one of the main concerns of researchers.

In recent years, a great amount of fault detection and isolation methods have been proposed for BLDCM that provide reliable health monitoring. Some researchers

proposed fault detection methods that are mainly based on system modelling [1, 2]; however, the fault detection accuracy depends on the accuracy of system modelling and the knowledge of system uncertainties. A different category of works named signal-based methods has been developed for condition monitoring of modules utilizing a measured crucial signal [3, 4].

An important research category in BLDCM has relied on data driven methods. Specially, artificial intelligence techniques have been receiving extensive attention. These methods do not require precise modelling and are not directly dependent on the measured signal conditions. Regarding this issue, a technique based on the radial basis function (RBF) neural network was proposed for the bearing and stator inter-turn faults [5]. The authors in [6]

presented a method based on a self-organizing map neural network for stator winding fault detection.

There are also hybrid methods that use the features of the signal processing approaches in combination with the artificial intelligence tools [7, 8]. The signal processing methods are adopted to obtain the fault features from the gathered data. These features are used as the input for machine learning classifiers like neural networks, fuzzy systems, or support vector machine (SVM) [9, 10]. Faults in BLDCM can cause extensive changes in different measurement signals, sometimes leading to complex relationship between the occurred faults and the affected parameters of these signals. Therefore, using the combination of features of the mentioned methods make it possible to obtain the above relationship more accurately. Papers [11] and [12] introduce bearing fault detection methods based on packet wavelet transform (PWT), the support vector machine (SVM) and the radial basis function (RBF) neural networks, respectively.

Some researchers have used different optimization algorithms to improve the efficiency and accuracy of intelligent methods. Some researchers have used PSO algorithm in order to improve neural network performance [13, 14]. Some researchers have introduced faults detection methods based on GA that improves performance of different kinds of neural networks [15, 16]. The other researchers have utilized grey wolf optimization (GWO) algorithm to improve accuracy of neural network classifiers [17, 18]. Although the reviewed methods have provided numerous and valuable features in the BLDCM fault detection and diagnosis, there are still some unresolved problems. In these methods, mainly one or a limited number of defects in the BLDCM have been covered and simultaneous occurrence of these defects is rarely considered. Besides, defects may occur in various loading conditions of motor that need to be predicted in advance. Also, all available and measurable signals are not used to classify defects more broadly.

Accordingly, a novel data-driven method is suggested in this paper to detect multiple defects including the stator inter-turn, the rotor dynamic imbalance, the rotor static imbalance and simultaneous occurrence of them. Unlike conventional methods, which mainly use current or vibration signals; the current signal is used together with the motor torque and the motor speed signal to achieve separability in the feature spaces. In the proposed method, the features of the aforementioned signals are extracted using the packet wavelet transform (PWT). These features, which include the energy in two modes of the BLDCM operation: without load and with load, serve as input to two types of neural networks, the radial basis function (RBF) neural network and the multilayer perceptron neural network. It is shown that the RBF neural network achieves more accurate classification results. To achieve a more effective performance, RBF weight coefficients are updated by the particle swarm optimization (PSO) and the genetic algorithm (GA) and then the results are compared.

The main contributions of this paper are: (1) A novel solution for multiple fault diagnosis is proposed that is compatible with simultaneous occurrence of defects (2) Unlike conventional methods, which mainly use current or vibration signals; the current signal is used together

with the motor torque and the motor speed signal which increases the ability to classify defects (3)The introduced method can be applied in both fixed and variant BLDC motor load conditions (3) The data-driven based fault detection and classification method is presented which does not require an accurate model of BLDC motor (4) The combination of data-driven method with optimization algorithms is introduced to achieve higher level of accuracy and performance of neural network (5) Packet wavelet transformation is used for feature extraction, which it is suitable for nonstationary signal analysis and does not require the use of any windows such as Fourier transformation. (7) The optimization algorithms are used to update the neural network weights that provide a quick and effective performance, better flexibility to local problems and more accurate results.

The paper structure is as follows: Sect. 2, introduces the fault diagnosis method. At the beginning of this section, the BLDCM model is represented. After that, the (SIT), (RSI) and (RDI) faults model are introduced. Next, the PWT and feature extraction method are shown. At the end of this section, the RBF neural network with PSO and GA algorithms is represented. In Sect. 3, the simulation results of proposed method are introduced. This section includes features extraction and neural network training simulation results. The Performance validation of the fault diagnosis method is introduced at the end of this section. Finally, the paper is concluded in Sect. 4.

## 2. The Fault Diagnosis Method

In this section, the design steps of the fault diagnosis method are described as shown in Fig. 1. In this figure, the BLDCM is simulated in different loading conditions in which several types of electromechanical faults are applied. The current, torque and speed signals of the BLDCM are measured and the features related to the above signals are extracted using the PWT. These features, which include the energy in the two modes of the BLDCM operation: without load and with load, are given as inputs to the RBF neural network. The neural network weighting coefficients are tuned by the PSO and the GA as optimization algorithms. As shown in Fig. 1, seven types of BLDCM faults are classified that include: stator inter-turn (SIT), rotor static imbalance (RSI), rotor dynamic imbalance (RDI), hybrid fault type 1 (SIT and RSI), hybrid fault type 2 (SIT and RDI), hybrid fault type 3 (RSI and RDI) and finally hybrid fault type 4 (SIT, RSI and RDI).

### 2.1. The BLDCM Model

In the BLDCMs, unlike the DC motors in which the brush is tasked with making a mechanical contact with the commutator, the connection is formed using a set of windings beside the permanent magnet between the stator and the rotor. The relations described below have been extracted based on the model adopted from [19]. The Phase-to-phase voltages of the BLDCM are given as:

$$V_{ab} = R(i_a - i_b) + L\frac{d}{dt}(i_a - i_b) + E_a - E_b \qquad (1)$$

$$V_{bc} = R(i_b - i_c) + L\frac{d}{dt}(i_b - i_c) + E_b - E_c \qquad (2)$$

$$V_{ac} = R(i_a - i_c) + L\frac{d}{dt}(i_a - i_c) + E_a - E_c \qquad (3)$$

where, the $L$ parameter is defined as $L = \ell - M$. Also, R is the motor resistance, $\ell$ is the self-inductance of the stator and $M$ is the mutual inductance of the stator. $i_a, i_b, i_c$ and $E_a, E_b, E_c$ are respectively, the stator currents and electromotive forces of phases a, b, and c. The mechanical equations of the BLDCM are as follows [20]:
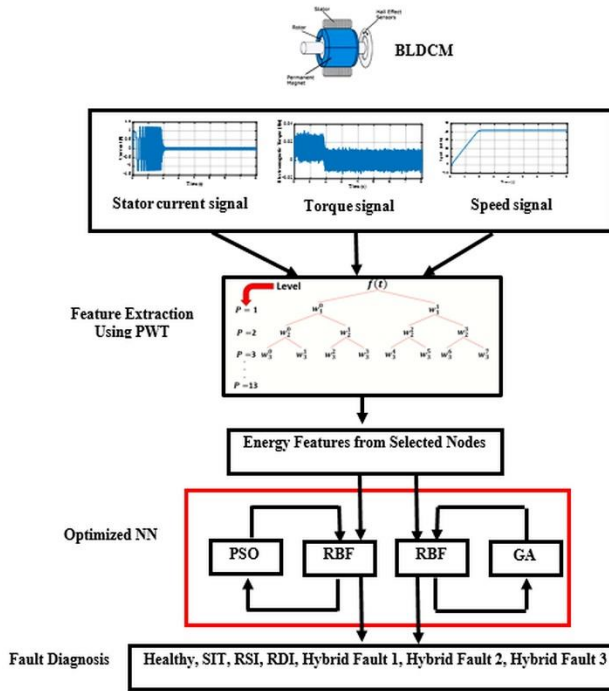


**Fig1.** Different steps of the proposed fault detection and classification method based on neural networks

$$T_e - T_l = J\frac{d^2\theta_m}{dt^2} + B\frac{d\theta_m}{dt} \qquad (4)$$

$$\theta_e = \frac{\mathcal{P}_{Rotor}}{2}\theta_m \qquad (5)$$

$$\omega_m = \frac{d\theta_m}{dt} \qquad (6)$$

where, $T_l$ and $J$ are the load torque and the moment of inertia of the rotor, respectively. The notations $\theta_m$, $B$ and $\mathcal{P}_{Rotor}$ represent the rotor position, the damping factor, and the number of motor poles, respectively. $\omega_m$ introduces the velocity of the rotor. The electrical torque of the BLDCM is given as:

$$T_e = K_T\left(F(\theta_e)\,i_a + F\left(\theta_e - \frac{2\pi}{3}\right)i_b + F\left(\theta_e + \frac{2\pi}{3}\right)i_c\right) \qquad (7)$$

where, $K_T = 2PN_sB_f lr$ is the constant torque, $F(\theta)$ is a trapezoidal function that builds the trapezoidal flux density form, $N_s$ is the number of winding rounds in each stator phase, $B_f$ is the average number of air space and $l$ and $r$ are the length and radius of the rotor, respectively. The load torque of the BLDCM is introduced as follows:

$$T_L = T_{DB} + T_{DF} \qquad (8)$$

where, $T_{DF}$ is the flywheel disturbance torque and $T_{DB}$ is the bearing disturbance torque, obtained from the sum of the coulomb and viscous frictions as follows:

$$T_{DB} = T_{viscouse} + T_{coulomb} = C_v\omega_m + C_c sign(\omega_m) \quad (9)$$

where $C_v$ and $C_c$ are viscous and coulomb friction coefficients, respectively. The back electromotive force on each phase of the stator windings is acquired as [21]:

$$E_a = K_e\omega_m F(\theta_e) \qquad (10)$$

$$E_b = K_e\omega_m F\left(\theta_e - \frac{2\pi}{3}\right) \qquad (11)$$

$$E_c = K_e\omega_m F\left(\theta_e + \frac{2\pi}{3}\right) \qquad (12)$$

where, $K_e$ is the induction electromotive constant. After arranging the above relationships, the BLDCM space state model is obtained as follows:

$$
\begin{pmatrix} \frac{di_a}{dt} \\ \frac{di_b}{dt} \\ \frac{d\omega}{dt} \\ \frac{d\theta_m}{dt} \end{pmatrix} = \begin{pmatrix} \frac{-R}{L} & 0 & 0 & 0 \\ 0 & \frac{-R}{L} & 0 & 0 \\ 0 & 0 & \frac{-B}{J} & 0 \\ 0 & 0 & 1 & 0 \end{pmatrix} \begin{pmatrix} i_a \\ i_b \\ \omega_m \\ \theta_m \end{pmatrix} +
$$
$$
\begin{pmatrix} \frac{2}{3L} & \frac{1}{3L} & 0 \\ \frac{-1}{3L} & \frac{1}{3L} & 0 \\ 0 & 0 & \frac{1}{J} \\ 0 & 0 & 0 \end{pmatrix} \begin{pmatrix} V_{ab} - E_{ab} \\ V_{bc} - E_{bc} \\ T_e - T_l \end{pmatrix} + D_{disturbance} \qquad (13)
$$

where $E_{ab} = E_a - E_b$ , $E_{bc} = E_b - E_c$ and $D_{disturbance}$ is disturbance. The current $i_c$ is calculated from (14) as:

$$i_c = -(i_a + i_b) \qquad (14)$$

### 2.2. The Stator Inter-Turn Fault Model

The stator faults form 28 % to 36 % of the motors faults [22]. Therefore, the issue of diagnosis of this defect is of particular importance. One of the causes of this defect, is the breakdown of the insulation between the rings. Fig. 2 shows how the stator winding loops can be shortened. It is assumed that the fault has occurred within the coil of phase a.
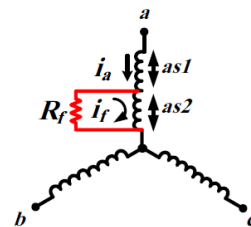


**Fig2**. Short inter-turn fault modelled in a 3-phase stator [23]

As shown in Fig. 2, *as1* is the healthy part of winding whereas *as2* is the shorted section of the winding. Also $i_a$ and $i_f$ show respectively the stator current and the circulating current induced due to the short connection [24]. Fig. 3a shows the stator winding model in healthy condition whereas Fig. 3b shows stator winding in faulty condition.
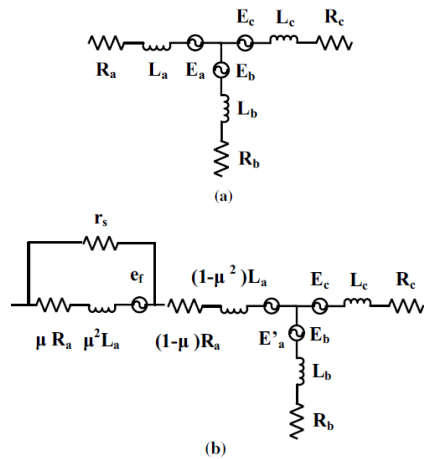
**Fig3.** The considered model for healthy and faulty stator (**a**) the healthy 3-phase stator (**b**) the faulty 3-phase stator

In Fig.3, $L_c, L_b, L_a$ , $R_c, R_b, R_a$ , $E_c, E_b$ and $E_a$ are inductances, resistances and back EMF of related stator phases respectively; besides, all "$R$" and "$L$" are considered equal to each other. "$e_f$" represents the back EMF obtained from the shorted circuit current; "$\mu$" indicates the ratio of short-circuit turns to the whole number of turns in one phase. Also, $r_s$ represents short-circuit impedance. In order to model the stator inter-turn short circuit, we must multiply the resistance and inductance of the healthy winding (Fig. 3a) into $(1 - \mu)$ and $(1 - \mu^2)$ respectively. Due to the stator short circuit inter-turn fault, some harmonics in the BLDCM signals are created with the below frequencies [23]:

$$f_{SIT} = (2k - 1)f_f \tag{15}$$

where, $k = 1,2,3 ...$ and $f_f$ is the fundamental frequency. In this paper, $f_f$ is considered as 20Hz so, the stator short circuit inter-turn frequencies are $f_{SIT} = 20,60,100,140 ...$ .

### 2.3. The Rotor Static and Dynamic Imbalance

In an ideal machine, the rotor rotation axis is exactly matched to the stator symmetry axis and the length of the air gap is the same everywhere. Rotor imbalance or in other words, rotor eccentricity is an uneven air gap between the stator and the rotor. Rotor eccentricity can happen in two ways, dynamic eccentricity, and static eccentricity. By static eccentricity, the position of the minimum radial air gap does not change and remains constant, in other words when the stator symmetry axis, $O_s$ , separates from the rotor symmetry axis, $O_r$ , and the rotor rotation axis, $O_w$ , static eccentricity occurs. The reasons that cause static eccentricity include the ellipsoid shape of the current or incorrect rotor position [25]. The dynamic eccentricity occurs when the rotor centre is not on the rotating centre of the rotor and the radial air gap rotates, in other words, when the rotor symmetry axis, $O_r$ , separates from the stator symmetry axis, $O_s$ , and the rotor rotation axis, $O_w$ , dynamic eccentricity occurs. The main reasons for dynamic eccentricity are shafts bending, mechanical resonance at critical speeds and bearing exhaustion [25]. When all three axes include: $O_r$ ,$O_s$ ,$O_w$

are separate from each other, the eccentricity is called the mixed eccentricity (static and dynamic eccentricity). Fig.4a illustrates the static eccentricity while Fig.4b and Fig.4c illustrate the dynamic and mixed eccentricities, respectively.
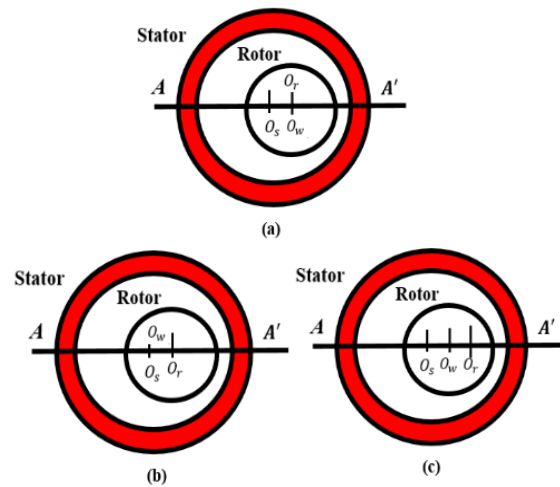


**Fig4.** The rotor dynamic and static imbalance faults (**a**) Static eccentricity (**b**) Dynamic eccentricity (**c**) Mixed eccentricity [26].

Eccentricities can be modelled according to the following relationships [27]:

$$\mathbf{F_s} = D_s \omega_W^2 \sin(\omega_W * t) \tag{16}$$
$$\mathbf{T_{DFS}} = R_W \times \mathbf{F_s} \tag{17}$$
$$\mathbf{T_{DFD}} = D_d \omega_W^2 \sin(\omega_W * t) \tag{18}$$

where, $t$ is time, $R_W$ is the wheel distance from the center of mass, $D_s$ is the static disturbance coefficient, $D_d$ is the dynamic disturbance coefficient, $\omega_W$ is the wheel speed, $\mathbf{T_{DFS}}$ and $\mathbf{T_{DFD}}$ are disturbance torques due to the static and dynamic eccentricity, respectively. Due to the static and dynamic eccentricities, some harmonics in the BLDCM signals are built with the below frequencies [28]:

$$f_{Dynamic} = f_f \left( 1 \pm \frac{k}{\mathcal{P}_{Poles}/2} \right) \tag{20}$$

$$f_{Static} = f_f \pm k f_r \tag{21}$$
$$f_r = \frac{\omega_r}{60} \tag{22}$$

where, $k = 1,2,3 ...$ and $\mathcal{P}_{Poles}$ is the number of motor poles. $f_r$ and $\omega_r$ are rotor frequency and speed, respectively. In this paper, The BLDCM has 6 poles with $\omega_r = 41.86 \, rad/sec$ desired rotor speed.

### 2.4. The Packet Wavelet Transform

Packet wavelet transform (PWT), is one of the methods of signal analysis in time-frequency domain. In this type of wavelet, in contrast to discrete wavelet transform which only approximate coefficients pass through low and high pass filters, both approximate (app.) and detail (det.) coefficients are passed through these filters for each step [29]. Fig. 5 shows how this type of wavelet works.

For $p$ levels of decomposition, the PWT produces $2^p$ different sets of coefficients called nodes.

The wavelet packet function can be introduced as follows [30]:

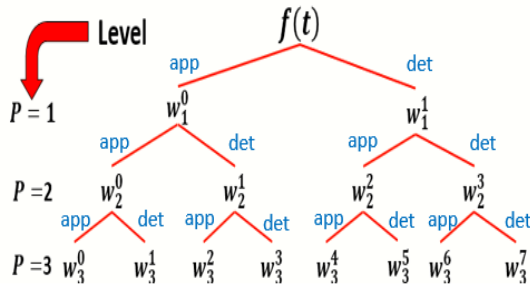$$W_{p,k}^m(t) = 2^{\frac{p}{2}} W^m(2^p t - k) \qquad (22)$$



**Fig5.** Packet wavelet transform tree at 3 levels with approximate and detail nodes.

where, *m* and *k* are operation modulation parameter and translation operations, respectively. PWT coefficients can be calculated according to the following relation:

$$w_{p,k}^m(t) = \langle f(t), W_{p.k}^m \rangle = \int f(t) W_{p.k}^m(t) dt \qquad (23)$$

where, $f(t)$ is main signal and operation $\langle f(t), W_{p.k}^m \rangle$ shows inner product of main signal and wavelet packet function. The nodes frequency intervals can be represented as below [30]:

$$((m-1)2^{-p-1}f_s, m2^{-p-1}f_s] \qquad (24)$$

where, $f_s$ is sampling frequency. For example, for 2 level of decomposition $2^2 = 4$ nodes are created and $w_2^0$ shows the 0th node in second level of decomposition. This node has $(0, \frac{f_s}{8}]$ frequency band. In the next section, the feature extraction using the mentioned coefficients are described.

### 2.5. Feature Extraction Using the Packet Wavelet Transform

PWT continues decomposition until a level where the frequency band of PWT coefficients consist of faults frequencies. PWT is applied to current, speed and torque signals of BLDCM in 4 different load conditions include: No-load (NL), Half-load (HL), Full-load (FL) and Decreased-load (DL). In this paper, the decomposition level is 13 and $2^{13}$ nodes can be produced for each signal in 4 different load conditions so $p = 13$ and $m = 0,1,2 \dots 2^{13} - 1$. Five nodes which includes: $w_{11}^0$, $w_{12}^0$, $w_{13}^0$, $w_{13}^1$ and $w_{13}^2$ are selected for feature extraction for each signal. Frequency band of these nodes consist fault frequencies. Energy of mentioned nodes in 4 different load conditions and 8 different fault conditions for each signal is selected as features and these features are given as input to the neural network for faults classify. The energy of mentioned nodes is calculated as follows [31]:

$$E_p^m = \sum_k \left( w_p^m(k) \right)^2 \qquad (25)$$

### 2.6. Radial Basis Function with Particle Swarm Optimization Algorithm

Particle swarm optimization is one of the evolutionary algorithms for optimization of different problems. This algorithm, is inspired by natural processes such as: mass migration of birds or mass movements of fishes. In this algorithm, a set of particles in the possible response space of the optimization function will start. Every particle in this space has a velocity and a position. Each particle, while remembering its best position in the space of response, sends its best position to the other particles and the other particles move toward that particle. At each iteration of this algorithm, the particles compare their current position with their best positions, $P_{best}$, and if the current value is better than $P_{best}$, it is replaced by $P_{best}$. By comparing the best position of each particle together, the best team position, $g_{best}$ is updated. The following relationships are used to update the position and speed of each particle [32]:

$$v_j(t+1) = \omega v_j(t) + c_1 r_1 \left( p_{best,j}(t) - p_j(t) \right) \qquad (26)$$
$$+ c_2 r_2 \left( g_{best,j}(t) - p_j(t) \right)$$
$$p_j(t+1) = p_j(t) + v_j(t+1) \qquad (27)$$

where, $p_j(t)$ and $v_j(t)$ are the position and velocity of the *i*th particle at the moment *t*, respectively, $\omega$ is the inertia coefficient, $c_1, c_2$ are learning coefficients and $r_1$ and $r_2$ are two positive parameters with values lower than one.

RBF neural networks are actually three-layer feedforward networks. In these networks, hidden layer neurons perform a set of radial basis functions while the output neurons have linear activating functions. Fig. 6 shows the structure of these networks.
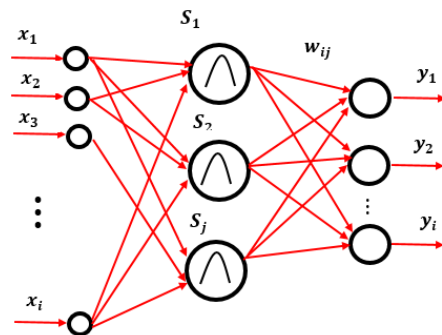


**Fig6.** RBF neural network structure with radial basis activation function [33]

As described in the previous section, the energy of the mentioned PWT coefficients $\left( E_p^m \right)$ in 4 different load conditions and 7 different fault conditions are given as input to the RBF neural network. RBF neural networks are based on supervised learning and its training algorithm can be divided into two phases: 1-Set the input layer weights to the hidden layer. 2-Set the hidden layer weights to the output layer.

In this paper, the RBF neural network can classify 7 different BLDCM faults. In healthy condition the RBF output shows number 1 while if it shows numbers 2, 3, 4, 5, 6, 7 and 8 it means that the BLDCM has RSI, SIT, RDI, Hybrid Fault 1, Hybrid Fault 2 and Hybrid Fault 3, respectively. Also, the RBF neural network output is calculated from the following equation:

$$y_i = \sum_{j=1}^{m} w_{ij}\, tanh\left(\, |x - s_j|^2 \right) \qquad (28)$$

As mentioned in section 2.5, $x$ is neural network inputs vector. $w_{ij}$ and $s_j$ are the hidden layer output weights and hidden layer centre points, respectively.

Multilayer perceptron (MLP) is feedforward neural network and another kind of supervised learning. This type of neural network has at least one hidden layer and one output layer. The MLP neural network output can be computed as follows:

$$y_i = f\left( \sum_{j=1}^{N} w_{ij}{}^{T} x_j + b_i \right) \qquad (29)$$

where, $x_j$ is neural network inputs vector. $w_{ij}$, $b_i$ and $f$ are the weights between the input number $i$ and neuron number $j$, bias and hidden layer activation function, respectively.

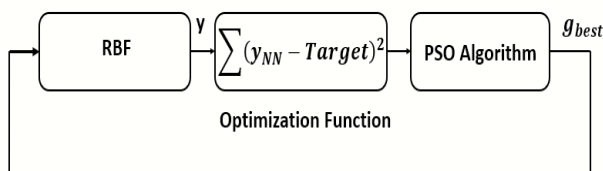In this paper, PSO algorithm is used to optimize the RBF neural network weights as shown in Fig.7.



**Fig7.** Block diagram of the RBF which weights updated with the PSO algorithm

As shown in Fig. 7, y and target are the RBF neural network output and the real class of inputs, respectively. The PSO optimization function is introduced as: $\sum(y - target)^2$. PSO algorithm based on equations (26) and (27) finds $g_{best}$ or best team position and it is used as RBF weights.

*2.7. Radial Basis Function with Genetic Algorithm*

Genetic algorithm is one of the meta-heuristic algorithms in optimal solution of different problems. This algorithm solves the optimization problems with the inspiration of nature and the formation of living organisms and converting these organisms into an optimal population. The general structure of the algorithm is shown in Fig. 8.
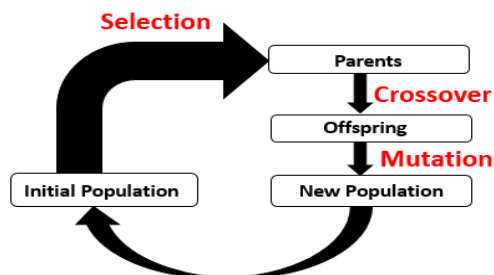


**Fig8**. Different steps of genetic algorithms

According to the above diagram, a number of population elements find the opportunity to reproduce.

Those elements chosen are called parents. In the crossover process, portions of the chromosomes are replaced and this makes children share their parent characteristics so children are different from their parents. This process goal is produce a new child with good qualities of its parents in order to produce a better creature. In the mutation process, a chromosome number is randomly chosen and then the values of one or more genes are changed. The mutation process produces a new population and it replaces with the previous population. The GA algorithm is repeated enough to achieve an optimal solution.

Function $\sum(y - target)^2$ is used as optimization function for GA algorithm. Where, y and target are RBF neural network output and real class of RBF neural network inputs, respectively. GA algorithm starts to find optimal solution for mentioned optimization function. The GA algorithm optimal solution is used as RBF neural network weights.

### 3. Simulation Results

In this section, the effectiveness of the proposed algorithms is validated. Fig. 9 shows the current signal of BLDC motor in healthy, stator inter-turn, static rotor imbalance, and dynamic rotor imbalance faults.
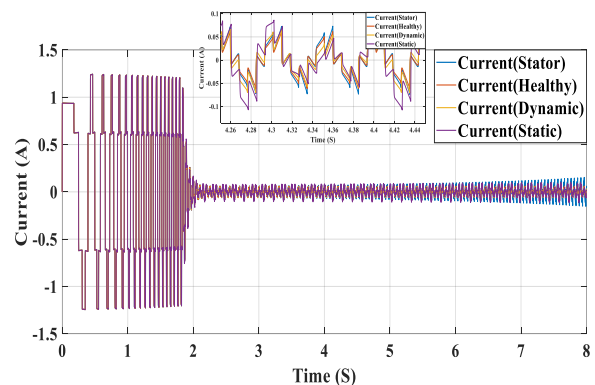


**Fig9**. The BLDC current in three faulty states (stator inter-turn, rotor static imbalances, and rotor dynamic imbalances) and healthy mode

For this purpose, the parameters for the BLDCM are considered as shown in Table I. Also, the selected parameters for the PSO and GA are represented in Table II and Table III, respectively.

**Table I.** The parameters of the BLDC motor MATLAB model

| Parameter | Value |
|---|---|
| Phase resistor | $8\Omega$ |
| Phase inductance | $2 \times 10^{-3} H$ |
| Phase inductance | $0.66 \times 10^{-3} kg.m^2$ |
| Damping coefficient | $2 \times 10^{-5} N.m.s/rad$ |
| Induction electromotive coefficient | $2 N.m/A$ |
| BLDC motor torque coefficient | $13.689 \times 10^{-3} N.m/A$ |
| Coulomb friction coefficient | $10^{-4} N.m$ |
| Viscous friction coefficient | $2 \times 10^{-5} N.m.s/rad$ |
| Sampling time | $5 \times 10^{-6} s$ |
| Dynamic imbalance disturbance coefficient | $3.6 \times 10^{-9}$ |
| Static imbalance disturbance coefficient | $9.2 \times 10^{-9}$ |
| Short-circuit impedance | $9 \times 10^{-3} \Omega$ |

**Table II.** The parameter related to the PSO algorithm

| Parameter | Value |
|---|---|
| Population Size (Swarm Size) | 100 |
| Inertia Weight | 0 |
| Inertia Weight Damping Ratio | 1 |
| Personal Learning Coefficient | 1.5 |
| Global Learning Coefficient | 2.0 |
| The Minimum Error | $10^{-20}$ |

**Table III.** The parameter related to the GA algorithm

| Parameter | Value |
|---|---|
| Initial Population Range | [-1,1] |
| Fitness Limit | 0 |
| The Minimum Error | $10^{-20}$ |

In the following, after explaining the different steps of feature extraction and neural network training, some test scenarios are considered for evaluating the designed algorithms.

*3.1. Feature Extraction*

By examining the Simulink model represented in Fig. 1, the current, electromechanical torque and speed signals are obtained in seven different fault scenarios. The energy features of the five selected nodes are extracted by the PWT (relation (23)). The large number of features ($2^{13} + 2^{12} + \cdots + 2^1$ ), for motor current, electromechanical torque and motor speed for each one of the BLDCM conditions including healthy, SIT, RSI, RDI, SIT and RSI, SIT and RDI, RSI and RDI and finally SIT, RSI and RDI in 3 different load levels include: No-load (NL), Half-load (HL), Full-load (FL) are considered.

These data are used as training and testing data for the neural network classifier, that is, 15 data sets for each of the motor conditions and for several load levels (NL, HL, FL). In general, there are 480 number of datasets, which 60 % of them are used for neural network training and 40 % of them are used for neural network testing.

*3.2. Neural Network Training*

As mentioned above, 1500 data sets have been intended for training the neural network in each of the BLDCM conditions. The RBF and MLP neural networks are evaluated to determine the best performance for fault diagnosis. Each neural network is developed with 3 neurons in the input layer, 1 neuron in the output layer and different neurons in the hidden layer. Fig. 10 shows the neural networks performance for different numbers of hidden neurons.
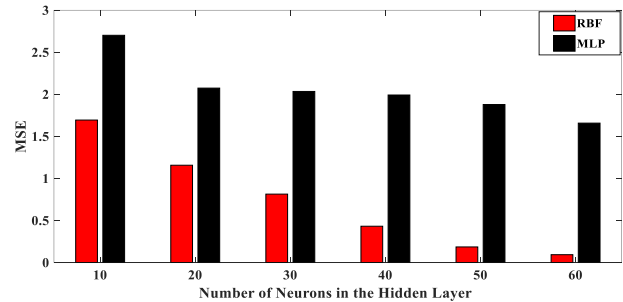


**Fig10** Neural networks performance for different neurons in hidden layer

As shown, the best performance of the RBF neural network is provided when the numbers of nodes in the hidden layer is 60 that achieves the mean square error (MSE) of 0.0930048. Also, 60 nodes in the hidden layer are required to provide the mean square error (MSE) of 1.6571 for the MLP neural network. Therefore, better performance for the data training step is obtained for the RBF neural network.

In order to achieve the best classification performance of the neural network, it is also required to obtain the most suitable parameters for the optimization algorithms, namely the PSO and the GA. To illustrate the impact of inertia weight, personal and general learning coefficients and inertia rate damping ratio for the PSO algorithm, the results for 4 different load conditions are represented in Table IV. In this table, Inertia Weight, Global Learning Coefficient, and Inertia Rate Damping Ratio named as IW, GLC, and IRDR for abbreviate purposes. In this table, the resulted MSE obtained for different values of PSO parameters have been illustrated. By consideration the mentioned factors, the values 0, 1.5, 2 and 1 are chosen respectively for inertia weight, personal and general learning coefficients and inertia rate damping ratio.

**Table IV.** PSO-RBF parameters Comparison based on MSE

| PSO-RBF Parameters | | MSE ($\times 10^{-22}$) | | | |
|---|---|---|---|---|---|
| | | NL | HL | FL | DL |
| IW | $w_{PSO} = 0$ | 6.635 | 2.525 | 1.221 | 7.465 |
| | $w_{PSO} = 1$ | 9.047 | 4.717 | 4.504 | 9.748 |
| | $w_{PSO} = 2$ | 9.985 | 6.695 | 5.437 | 10. 44 |
| | $w_{PSO} = 5$ | 11.30 | 7.683 | 6.894 | 11.96 |
| GLC | $\begin{cases} c_1 = 2 \\ c_2 = 2 \end{cases}$ | 6.429 | 4.171 | 2.601 | 8.488 |
| | $\begin{cases} c_1 = 1.5 \\ c_2 = 2 \end{cases}$ | 5.342 | 3.026 | 2.058 | 6.945 |
| | $\begin{cases} c_1 = 2.8 \\ c_2 = 1.3 \end{cases}$ | - | - | - | - |
| IRDR | $w_{Damp} = 0.5$ | 5.593 | 4.992 | 2.764 | 6.135 |
| | $w_{Damp} = 0.99$ | 4.670 | 3.307 | 2.441 | 5.611 |
| | $w_{Damp} = 1$ | 3.081 | 2.878 | 2.071 | 4.403 |

According to Table V, the value [0;1] chosen for the initial population range parameter in the GA result in the most appropriate performance. To illustrate the impact of inertia weight, personal and general learning coefficients and inertia rate damping ratio for the PSO algorithm, the results for 4 different load conditions based on convergence time are represented in Table V.

**Table V.** PSO-RBF parameters Comparison based on Convergence Time

| PSO-RBF Parameters | | Convergence Time | | | |
|---|---|---|---|---|---|
| | | NL | HL | FL | DL |
| IW | $w_{PSO} = 0$ | 55 | 56 | 58 | 59 |
| | $w_{PSO} = 1$ | 154 | 156 | 161 | 157 |
| | $w_{PSO} = 2$ | 225 | 226 | 225 | 224 |
| | $w_{PSO} = 5$ | 319 | 317 | 319 | 316 |
| GLC | $\begin{cases} c_1 = 2 \\ c_2 = 2 \end{cases}$ | 60 | 65 | 72 | 63 |
| | $\begin{cases} c_1 = 1.5 \\ c_2 = 2 \end{cases}$ | 56 | 57 | 55 | 55 |
| | $\begin{cases} c_1 = 2.8 \\ c_2 = 1.3 \end{cases}$ | - | - | - | - |
| IRDR | $w_{Damp} = 0.5$ | 56 | 55 | 56 | 53 |
| | $w_{Damp} = 0.99$ | 56 | 57 | 59 | 58 |
| | $w_{Damp} = 1$ | 54 | 53 | 54 | 56 |

**Table VI.** GA-RBF parameter Comparison

| GA-RBF Parameters | | Initial Population Range | | | |
|---|---|---|---|---|---|
| | | [0; 1] | [−1; 1] | [−5; 5] | [−10; 10] |
| MSE ($\times 10^{-4}$) | NL | 0.120 | 0.137 | 0.356 | 0.160 |
| | HL | 0.227 | 0.354 | 0.957 | 0.217 |
| | FL | 0.360 | 1.730 | 1.890 | 0.345 |
| | DL | 6.946 | 9.517 | 12 | 5.496 |
| Convergence Time (Iteration) | NL | 0.160 | 348 | 508 | 465 |
| | HL | 0.217 | 400 | 551 | 307 |
| | FL | 0.345 | 648 | 631 | 545 |
| | DL | 5.496 | 579 | 571 | 566 |

According to Table VI, the value [0;1] chosen for the initial population range parameter in the GA result in the most appropriate performance.

As shown in these tables, the best performance is achieved by combination of RBF neural network and the PSO algorithm. In the next section, the aforementioned combination of algorithms is further evaluated using different test data.

### 3.3. Performance Validation of The Fault Diagnosis Method

In this section, the results of the diagnostic algorithm for the validation stage are illustrated. For this purpose, the following test scenarios are selected considering different conditions of the BLDCM:

- Case 1: Static imbalance starts at time t=2.
- Case 2: Stator inter-turn, static and dynamic imbalances occur simultaneously at time t= 7 with $\mu = 0.75$.

**Case 1**

The results of the fault diagnosis for the PSO- RBF and the GA-RBF methods are shown in Table VII. As indicated in this table, the investigated networks achieve acceptable MSE and convergence time in different loading levels. However, the better value of performance is obtained by the PSO that provides more accurate results in less convergence time.

**Table VII.** The obtained MSE and convergence time of the proposed methods in Case 1

| Algorithms | | PSO-RBF | GA-RBF |
|---|---|---|---|
| MSE ($\times 10^{-9}$) | NL | 0.14603 | 5445 |
| | HL | 9.3679 | 250400 |
| | FL | 117.78 | 525.2578 |
| | DL | 1.4972 | 11273 |
| Convergence Time (Iteration) | NL | 65 | 235 |
| | HL | 85 | 285 |
| | FL | 80 | 595 |
| | DL | 78 | 319 |

**Case 2**

The results of the fault diagnosis for the PSO- RBF and the GA-RBF methods are shown in Table VIII.

According to this table, acceptable performance is achieved again by the proposed algorithms. However, the convergence time of the PSO- RBF is less, while it obtains better MSE results.

**Table VIII.** The obtained MSE and convergence time of the proposed methods in Case 2

| Algorithms | | PSO-RBF | GA-RBF |
|---|---|---|---|
| MSE ($\times 10^{-6}$) | NL | 0.021564 | 8.2230 |
| | HL | 0.064532 | 26.261 |
| | FL | 0.088965 | 2.5686 |
| | DL | 0.067658 | 54.714 |
| Convergence Time (Iteration) | NL | 49 | 609 |
| | HL | 72 | 377 |
| | FL | 48 | 382 |
| | DL | 106 | 251 |

The results indicated an acceptable performance with high classification accuracy that is attributed to the selected signals for measurement and the approach used to extract the features. In order to show the effectiveness and accuracy of the proposed method for seven different faults detection and classification, Fig. 11 shows the accuracy and percentage of false classification with confusion matrix.
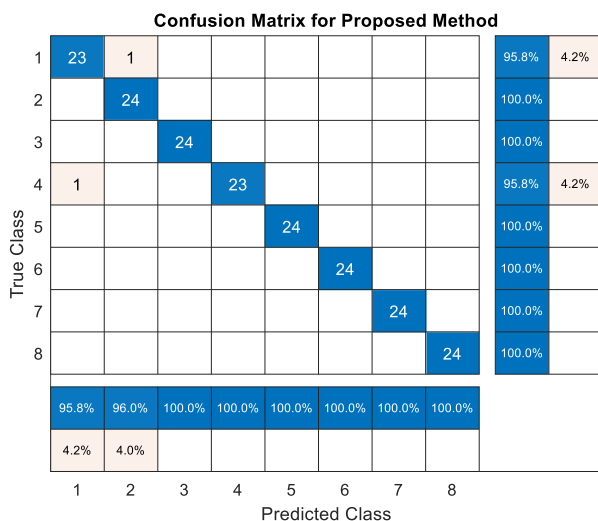


**Fig 11** Confusion matrix that compare the results of fault detection in healthy and seven different faulty modes of BLDC motor

In healthy condition the true class shows number 1 while if it shows numbers 2, 3, 4, 5, 6, 7 and 8 it means that the BLDCM has static rotor eccentricity, stator inter-turn, dynamic rotor eccentricity, simultaneous occurrence of stator inter-turn and static rotor eccentricity, simultaneous occurrence of stator inter-turn and dynamic rotor eccentricity, simultaneous occurrence of static rotor eccentricity and dynamic rotor eccentricity and simultaneous occurrence of all mentioned faults, respectively. Consequently, the classification strategy

based on the proposed methods resulted in an acceptable degree of generalization. For more comparison, Fig. 12 compares the accuracy obtained by the proposed method (PSO-RBF) with work done in [34] for BLDCM in SIT fault condition. In [34], the discreet wavelet transform (DWT) has been used as feature extraction and the multi-layer perceptron (MLP) neural network has been introduced as classifier in order to detect stator inter-turn short circuit fault. The energy Eigen value of 3 phases motor stator current in different fault and load conditions is used as MLP neural network inputs. The MLP neural network is trained by back propagation (BP) algorithm.
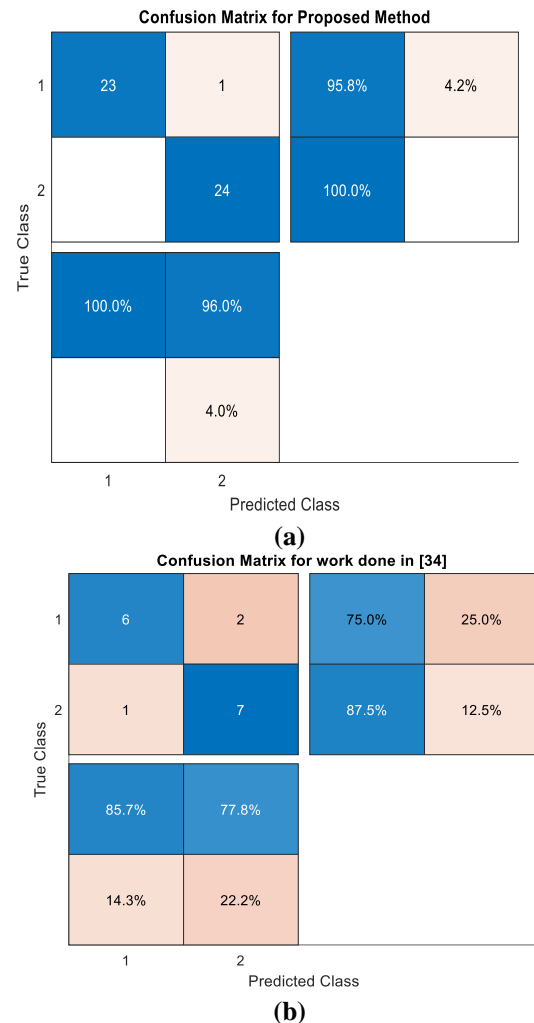


(a)



(b)

**Fig 12** (a) Confusion matrixes for proposed method (b) Confusion matrixes for the work done in [34]

As shown in Fig. 12, confusion matrix for the presented method and the work done in paper [34] shown in part (a) and (b), respectively. For better comparison, both confusion matrices are shown for stator inter-turn fault. In confusion matrix (a), test data include 48 data while, test data for confusion matrix (b) include 16 data. As shown in this figure, better performance of the proposed method is established compared to the mentioned related method. Utilizing radial basis function neural network has many advantages that mentioned before, however, it has still

problems in order to determine the hyper-parameters such as the number of hidden layers and the number of nodes in each layer. Furthermore, the proposed method is based on data-driven methods and it requires data sets in order to train the radial basis function neural network.

According to the authors experiences, this work can be improved by utilizing different ideas: In order to tackle with determining the hyper-parameters of neural networks, increase the number of hidden layers of neural network and use deep neural network can be a good solution for the future works. In addition, increasing the performance and efficiency of the deep neural network by tackling missing data and big noises problems can improved the accuracy of fault classification method. Besides, collecting the training data from real time prototype which will need some pieces of equipment such as high accuracy sensors, obtaining an accurate nonlinear model of the BLDC motor by using neural networks, considering different variant load conditions in the simulation scenarios, and the experimental validation of the total method would be great suggestions for future works.

## 4. Conclusion

In this article, a fault diagnosis method is proposed to classify multiple faults of different BLDCM conditions (SIT, RSI and RDI). The current signal was considered together with the electromechanical torque and motor speed as diagnostic media. The above measurements were used to extract energy features by the PWT and it was shown that an acceptable isolation capability is achieved. The extracted features for different BLDCM conditions and loading levels serve as inputs for the neural network-based classifiers. Also, the PSO and GA were suggested as optimization methods to update the neural networks weightings. It was shown that the convergence time of RBF-PSO is less, while it achieves more accurate results. For further evaluation of the proposed method, some test cases were considered. It was confirmed that the designed algorithm is effective that gives the required classification accuracy with acceptable convergence time. Therefore, the developed diagnosis features and the considered combination of neural networks with the PWT approach allow multiple diagnosis of BLDCM faults that occur in different operating conditions. The paper can be improved by considering the BLDC motor in different variant load mode in order to enhance the performance of the method in the future works and propose the fault detection and classification method which can be used in indifferent variant load conditions.

## References

1.     Eissa, M.A., et al. Improved fuzzy Luenberger observer-based fault detection for BLDC motor. in 2015 Tenth International Conference on Computer Engineering & Systems (ICCES). 2015. IEEE.

2.     El Mekki, A. and K.B. SAAD, Diagnosis based on a sliding mode observer for an inter-turn short circuit fault in brushless dc motors. Revue Roumaine des Sciences Techniques-Electrotechnique et Energétique, 2018. 63(4): p. 391-396.

3.     Guezmil, A., et al., Detecting inter-turn short-circuit fault in induction machine using high-order sliding mode observer: simulation and experimental verification. Journal of Control, Automation and Electrical Systems, 2017. 28(4): p. 532-540.

4.     Zandi, O. and J. Poshtan. Brushless DC motor bearing fault detection using Hall effect sensors and a two-stage wavelet transform. in Electrical Engineering (ICEE), Iranian Conference on. 2018. IEEE.

5.     Abd Alla, A.N., Three phase induction motor faults detection by using radial basis function neural network. Journal of applied sciences, 2006. 6(13): p. 2817-2820.

6.     Chuang, C., et al., The diagnosis method of stator winding faults in PMSMs based on SOM neural networks. Energy Procedia, 2017. 105: p. 2295-2301.

7.     Yuan, L., et al., Rolling bearing fault diagnosis based on convolutional neural network and support vector machine. IEEE Access, 2020. 8: p. 137395-137406.

8.     Lee, C.-Y. and T.-A. Le, Optimised approach of feature selection based on genetic and binary state transition algorithm in the classification of bearing fault in BLDC motor. IET Electric Power Applications, 2020. 14(13): p. 2598-2608.

9.     Ray, S., B. Ganguly, and D. Dey, Identification and Classification of Stator Inter-Turn Faults in Induction Motor Using Wavelet Kernel Based Convolutional Neural Network. Electric Power Components and Systems, 2020: p. 1-16.

10.    Yan, X. and M. Jia, A novel optimized SVM classification algorithm with multi-domain feature and its application to fault diagnosis of rolling bearing. Neurocomputing, 2018. 313: p. 47-64.

11.    Yadav, O.P. and G. Pahuja, Bearing Fault Detection Using Logarithmic Wavelet Packet Transform and Support Vector Machine. International Journal of Image, Graphics & Signal Processing, 2019. 11(5).

12.    Zhou, J., et al., Evaluation of Rolling Bearing Performance Degradation Using Wavelet Packet Energy Entropy and RBF Neural Network. Symmetry, 2019. 11(8): p. 1064.

13.    Deng, W., et al., A novel intelligent diagnosis method using optimal LS-SVM with improved PSO algorithm. Soft Computing, 2019. 23(7): p. 2445-2462.

14.    Yektaniroumand, T., M. Niaz Azari, and M. Gholami, Optimal rotor fault detection in induction motor using particle-swarm optimization optimized neural network. International Journal of Engineering, 2018. 31(11): p. 1876-1882.

15.    Xiong, J., et al., Combining the multi-genetic algorithm and support vector machine for fault diagnosis of bearings. Shock and Vibration, 2018. 2018.

16.    Zhu, X., J. Xiong, and Q. Liang, Fault diagnosis of rotation machinery based on support vector machine optimized by quantum genetic algorithm. IEEE Access, 2018. 6: p. 33583-33588.

17.    Huang, H., et al., An intelligent fault identification method of rolling bearings based on SVM optimized by improved GWO. Systems Science & Control Engineering, 2019. 7(1): p. 289-303.

18.    Li, L.-L., et al., Fault Diagnosis of High-Speed Brushless Permanent-Magnet DC Motor Based on Support Vector Machine Optimized by Modified Grey Wolf Optimization Algorithm. Symmetry, 2021. 13(2): p. 163.

19.    Baldursson, S., Bldc motor modelling and control-a matlab®/simulink® implementation. 2005.

20.    Hanselman, D.C., Brushless permanent magnet motor design. 2003: The Writers' Collective.

21.    Jeon, Y., et al. A new simulation model of BLDC motor with real back EMF waveform. in COMPEL 2000. 7th Workshop on Computers in Power Electronics. Proceedings (Cat. No. 00TH8535). 2000. IEEE.

22.    Sardana, G., N. Turk, and S. Deswal, Detection of Stator Winding Faults Using Finite Element Analysis (FEA) in BLDC Motors.

23.    Park, J.-K. and J. Hur, Detection of inter-turn and dynamic eccentricity faults using stator current frequency pattern in IPM-type BLDC motors. IEEE Transactions on Industrial Electronics, 2015. 63(3): p. 1771-1780.

24.    Kim, K.-T., S.-T. Lee, and J. Hur, Diagnosis technique using a detection coil in BLDC motors with interturn faults. IEEE transactions on magnetics, 2014. 50(2): p. 885-888.

25.      *Rajagopalan, S., et al., Analytic-wavelet-ridge-based detection of dynamic eccentricity in brushless direct current (BLDC) motors functioning under dynamic operating conditions. IEEE Transactions on Industrial Electronics, 2007. **54**(3): p. 1410-1419.*

26.      *Faiz, J. and M. Ojaghi, Different indexes for eccentricity faults diagnosis in three-phase squirrel-cage induction motors: A review. Mechatronics, 2009. **19**(1): p. 2-13.*

27.      *Liu, L., Jitter and basic requirements of the reaction wheel assembly in the attitude control system. Massachusetts Institute of Technology, 2007.*

28.      *Akar, M., Detection of a static eccentricity fault in a closed loop driven induction motor by using the angular domain order tracking analysis method. Mechanical Systems and Signal Processing, 2013. **34**(1-2): p. 173-182.*

29.      *Zarei, J. and J. Poshtan, Bearing fault detection using wavelet packet transform of induction motor stator current. Tribology International, 2007. **40**(5): p. 763-769.*

30.      *Wu, J.-D. and C.-H. Liu, An expert system for fault diagnosis in internal combustion engines using wavelet packet transform and neural network. Expert systems with applications, 2009. **36**(3): p. 4278-4286.*

31.      *Sun, Q., et al. Fault diagnosis of SEPIC converters based on PSO-DBN and wavelet packet energy spectrum. in 2017 Prognostics and System Health Management Conference (PHM-Harbin). 2017. IEEE.*

32.      *Bai, Q., Analysis of particle swarm optimization algorithm. Computer and information science, 2010. **3**(1): p. 180.*

33.      *Asfani, D.A., et al., Temporary short circuit detection in induction motor winding using combination of wavelet transform and neural network. Expert Systems with Applications, 2012. **39**(5): p. 5367-5375.*

34.      *Bessam, B., et al., Wavelet transform and neural network techniques for inter-turn short circuit diagnosis and location in induction motor. International Journal of System Assurance Engineering and Management, 2017. **8**(1): p. 478-488.*